Liquid Crystals
Publication details, including instructions for authors and subscription information:
http://www.informaworld.com/smpp/title~content=t713926090

Nature-inspired light-harvesting liquid crystalline porphyrins for organic photovoltaics

Lanfang Li[a]; Shin-Woong Kang[b]; John Harden[a]; Qingjiang Sun[c]; Xiaoli Zhou[a]; Liming Dai[c]; Antal Jakli[a]; Satyendra Kumar[bd]; Quan Li[a]
[a] Liquid Crystal Institute, Kent State University, Kent, OH 44240, USA [b] Department of Physics, Kent State University, Kent, OH 44240, USA [c] Department of Chemical and Materials Engineering, University of Dayton, Dayton, OH 45469, USA [d] Division of Materials Research, National Science Foundation, Arlington, VA 22230, USA

To cite this Article Li, Lanfang , Kang, Shin-Woong , Harden, John , Sun, Qingjiang , Zhou, Xiaoli , Dai, Liming , Jakli, Antal , Kumar, Satyendra and Li, Quan(2008) 'Nature-inspired light-harvesting liquid crystalline porphyrins for organic photovoltaics', Liquid Crystals, 35: 3, 233 — 239
To link to this Article: DOI: 10.1080/02678290701806584
URL: http://dx.doi.org/10.1080/02678290701806584

Liquid Crystals,
Vol. 35, No. 3, March 2008, 233–239

Taylor & Francis
Taylor & Francis Group

Nature-inspired light-harvesting liquid crystalline porphyrins for organic photovoltaics

Lanfang Li[a], Shin-Woong Kang[b], John Harden[a], Qingjiang Sun[c], Xiaoli Zhou[a], Liming Dai[c], Antal Jakli[a], Satyendra Kumar[bd] and Quan Li[a]*

[a]*Liquid Crystal Institute, Kent State University, Kent, OH 44240, USA;* [b]*Department of Physics, Kent State University, Kent, OH 44240, USA;* [c]*Department of Chemical and Materials Engineering, University of Dayton, Dayton, OH 45469, USA;* [d]*Division of Materials Research, National Science Foundation, 4201 Wilson Blvd., Arlington, VA 22230, USA*

(Received 3 October 2007; accepted 5 November 2007)

A new class of nanoscale light-harvesting discotic liquid crystalline porphyrins, with the same basic structure of the best photoreceptor in nature (chlorophyll), was synthesized. These materials can be exceptionally aligned into a highly ordered architecture in which the columns formed by intermolecular π–π stacking are spontaneously perpendicular to the substrate. The homeotropic alignment, well confirmed by synchrotron X-ray diffraction, could not only provide the most efficient pathway for hole conduction along the columnar axis crossing the device thickness, but also offer the largest area to the incident light for optimized light harvesting. Their preliminary photocurrent generation and photovoltaic performances were also demonstrated. The results provide new and efficient pathways to the development of organic photovoltaics by using homeotropically aligned liquid crystal thin films.

Keywords: nature-inspired liquid crystals; light-harvesting porphyrin; hexagonal phase; homeotropic alignment; photovoltaics

1. Introduction

Energy directly generated from sunlight will be a key energy solution for the new era, with photovoltaic technology offering a viable alternative to the ever-depleting supply of fossil fuels. A main challenge in converting solar energy into electrical energy is to develop inexpensive and efficient organic photovoltaic (OPV) materials and systems with satisfactory performance (*1–5*). The crystalline silicon photovoltaic cells, though efficient, appear too expensive to compete with primary fossil energy. The OPV technology would hold a promise for cost reduction since the OPV materials are potentially cheap, easy to process and capable of being deposited on flexible substrates and bent, whereas their inorganic competitors, e.g. crystalline silicon, would crack (*2*). However, currently widely used OPV materials, e.g. polycrystalline Cu phthalocyanine, suffer from electron/exciton scattering at grain boundaries resulting in poor charge mobility. A challenge for OPV materials with the possibility of significant cost reduction is to make them in a desired macroscopic order to improve charge transportation. One route to accomplish this goal is to induce a liquid crystalline phase in efficient OPV materials since liquid crystals (LCs) can respond easily to external stimuli and their alignment can be manipulated by external fields and surface effects (*6*). Among all LCs, the discotic LCs having superior absorption in solar energy bands and capable of being homeotropically aligned (i.e. the columns formed by intermolecular strong π–π self-assembly are perpendicular to the electrode surface) would be the desirable candidate to meet this challenge. Unfortunately, the homeotropic alignment of such discotic LCs is difficult to achieve due to high viscosity, although the alignment technology of rod-shaped LCs is well established in the liquid crystal display industry (*6, 7*).

For efficient absorption of sunlight it is logical to use porphyrin as the building block of discotic materials since it has the basic structure of the best photoreceptor in nature, chlorophyll. Porphyrin and its derivatives have many desirable features, such as highly conjugated disc plane, high stability, efficient absorption of sunlight and a small gap between the highest occupied molecular orbital (HOMO) and lowest unoccupied molecular orbital (LUMO) energy levels (*8*). The first porphyrin-based LC was synthesized in 1980 (*9*). However, an impressive example of liquid crystalline porphyrins and their potential for use in organic electronic material was reported by Bard and co-workers in 1989 (*10*). Unfortunately, research on these materials did not progress well due to their extremely difficult synthesis (*11*).

In this paper, we report a new class of nanoscale discotic liquid crystalline porphyrins which have a unique structure, i.e. twelve flexible chains around a porphyrin core. These materials can be exceptionally

*Corresponding author. Email: quan@lci.kent.edu

ISSN 0267-8292 print/ISSN 1366-5855 online

DOI: 10.1080/02678290701806584
http://www.informaworld.com

homeotropically aligned. The general structure shown in Figure 1 has not been reported previously.

2. Experimental

Materials and methods

All chemicals and solvents were purchased from commercial suppliers and used without further purification. Melting points are uncorrected. ^{1}H NMR and ^{13}C NMR spectra were recorded in $CDCl_3$. Chemical shifts, δ, are in ppm units, with the residual solvent peak as the internal standard. NMR splitting patterns are designated as follows: brs, broad singlet; s, singlet; d, doublet; t, triplet; m, multiplet. Column chromatography was carried out on silica gel (60–200 mesh). Analytical thin layer chromatography (TLC) was performed on commercially coated 60 mesh F_{254} glass plates. Spots were rendered visible by exposing the plate to UV light. Elemental analysis was performed by Robertson Microlet Inc. Infrared FT-IR spectra were recorded with a KBr pellet. Textures and transition temperatures of the target compounds were observed by polarizing optical microscopy (POM) using a Leitz microscope in conjunction with a Linkam TMS temperature controller. Calorimetric measurements were performed in a Perkin Elmer differential scanning calorimeter using indium as a standard calibration. For the conventional powder diffractions, the sample was loaded into 1.5 mm diameter Lideman capillary and exposed to synchrotron X-ray source of the advanced photon source (APS) at Argonne National Laboratory (Midwestern University Collaborative Access Team's facilities on Sector 6). An X-ray wavelength of 0.76533 Å was used. The diffraction patterns were recorded at different temperatures during cooling from the isotropic phase using a high-resolution MAR3450 area detector placed at a distance of 527.8 mm from the sample. The data were calibrated against a silicon standard (NIST 640C) and analysed using the software package FIT2D developed by A.P. Hammersley of the European Synchrotron Radiation Facility. For homeotropically aligned porphyrin-based LCs, the samples were sandwiched between 50 μm thick bare glass plates with an 8.0 μm gap. Microdiffraction experiments were performed using 16 keV X-rays at the bending magnet beamline of Sector 20 at the APS. The X-ray beam was focused to a 14×14 μm size using Kikpartrick–Baez mirrors. The sample cell was mounted inside a hot stage that controlled the sample temperature to $\pm 0.02^{\circ}$C (*12*).

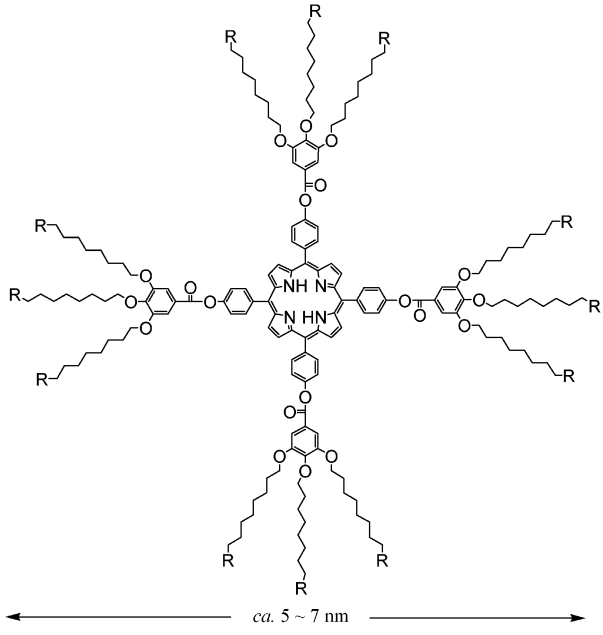

1 R=H; **2** R=CH_2CH_3; **3** R=$(CH_2)_3CH_3$; **4** R=$(CH_2)_5CH_3$; **5** R=$(CH_2)_7CH_3$

Figure 1. Molecular structures of the porphyrins **1**–**5**.

Characterization

The chemical structures of the target porphyrins **1**–**5** were well identified by ^{1}H NMR, ^{13}C NMR, IR and elemental analysis.

For **1**, ^{1}H NMR ($CDCl_3$): δ −2.05 (brs, 2H), 0.91 (t, 36H), 1.32 (m, 120H), 1.91 (m, 24H), 4.16 (m, 24H), 7.60 (s, 8H), 7.64 (d, J=8.2 Hz, 8H), 8.29 (d, J=8.2 Hz, 8H), 8.95 (s, 8H). ^{13}C NMR: 14.08, 22.68, 26.09, 26.15, 29.30, 29.39, 29.54, 30.41, 31.85, 31.92, 69.46, 73.69, 108.92, 119.93, 120.15, 123.99, 131.27, 135.39, 139.64, 143.41, 151.12, 153.15, 165.22. IR (KBr, ν_{max} in cm^{-1}): 2925.31, 2854.19, 1737.02, 1586.96, 1501.27, 1467.29, 1430.27, 1336.01, 1232.00, 1193.32, 1164.89, 1116.43, 1019.84, 994.47, 967.15, 951.45, 862.48, 801.25, 751.48.

For **2**, ^{1}H NMR ($CDCl_3$): δ −2.05 (brs, 2H), 0.90 (t, 36H), 1.31 (m, 168H), 1.91 (m, 24H), 4.16 (m, 24H), 7.60 (s, 8H), 7.64 (d, J=8.8 Hz, 8H), 8.30 (d, J=8.8 Hz, 8H), 8.95 (s, 8H). ^{13}C NMR: 14.09, 22.70, 26.12, 26.16, 29.37, 29.41, 29.44, 29.61, 29.67 29.76, 30.42, 31.94, 69.46, 73.69, 108.92, 119.33, 120.15, 123.99, 131.27, 135.39, 139.65, 143.41, 151.13, 153.15, 165.22. IR (KBr, ν_{max} in cm^{-1}): 2921.36, 2851.48, 1736.12, 1587.43, 1503.27, 1466.17, 1457.06, 1386.45, 1337.00, 1198.07, 1166.31, 1119.58, 1019.85, 961.88, 860.65, 796.03, 751.70, 724.57. Elemental analysis: calculated for $C_{192}H_{286}N_4O_{20}$, C 77.64, H 9.70, N 1.89; found, C 77.44, H 9.70, N 2.06.

For **3**, ^{1}H NMR ($CDCl_3$): δ −2.77 (brs, 2H), 0. 90 (t, 36H), 1.29 (m, 216H), 1.88 (m, 24H), 4.16(m, 24H), 7.61 (s, 8H), 7.67 (d, J=8.6 Hz, 8H), 8.30 (d, J=8.6 Hz, 8H), 8.96 (s, 8H). ^{13}C NMR: 14.09, 22.70,

26.16, 29.37, 29.41, 29.46, 29.68, 29.72, 29.77, 30.43, 31.94, 69.47, 73.67, 108.92, 119.34, 120.16, 124.00, 131.28, 135.40, 139.65, 143.41, 151.13, 153.16, 165.22. IR (KBr, ν_{max} in cm^{-1}): 2920.07, 2850.22, 1736.26, 1587.40, 1502.87, 1467.16, 1457.13, 1429.72, 1387.15, 1336.54, 1197.01, 1166.24, 1119.80, 1019.62, 964.97, 867.02, 796.27, 752.10, 724.07. Elemental analysis: calculated for $C_{216}H_{334}N_4O_{20}\cdot H_2O$, C 78.02, H 10.19, N 1.69; found, C 78.03, H 10.18, N 1.58.

For **4**, ^{1}H NMR ($CDCl_3$): δ −2.77 (brs, 2H), 0.88 (t, 46H), 1.28 (m, 240H), 1.87 (m, 24H), 4.16 (m, 24H), 7.60 (s, 8H), 7.64 (d, J=8.2 Hz, 8H), 8.29 (d, J=8.2 Hz, 8H), 8.95 (s, 8H). ^{13}C NMR: 14.08, 22.68, 26.12, 26.16, 29.36, 29.39, 29.42, 29.46, 29.68, 29.72, 29.76, 30.43, 31.93, 69.47, 73.69, 77.20, 108.92, 119.33, 120.16, 123.99, 131.29, 135.39, 139.65, 143.39, 151.12, 153.15, 165.22. IR (KBr, ν_{max} in cm^{-1}): 2921.73, 2851.65, 1736.61, 1587.08, 1502.80, 1467.02, 1429.92, 1386.40, 1336.15, 1194.08, 1166.15, 1119.17, 1019.49, 967.06, 861.95, 796.87, 752.27, 723.69.

For **5**, ^{1}H NMR ($CDCl_3$): δ −2.77 (brs, 2H), 0.88 (t, 9H), 1.27 (m, 264H), 1.87 (m, 43H), 4.16 (m, 32H), 7.60 (s, 8H), 7.64 (d, J=8.6 Hz,, 8H), 8.29 (d, J=8.6 Hz, 8H), 8.95 (s, 8H). ^{13}C NMR: 14.07, 22.67, 26.17, 29.35, 29.46, 29.68, 29.72, 30.43, 31.92, 69.75, 73.70, 108.94, 119.33, 120.16, 124.00, 131.34, 135.40, 139.65, 143.42, 151.13, 153.16, 165.22. IR (KBr, ν_{max} in cm^{-1}): 2919.43, 2850.74, 1737.49, 1587.18, 1501.75, 1467.78, 1430.39, 1384.32, 1336.01, 1193.05, 1166.92, 1118.78, 1019.43, 967.43, 798.77, 721.81, 673.26.

3. Results and discussion

The porphyrins **1**–**5** are thermally stable even at 300°C. Their phase behavior was investigated by crossed-polarized optical microscopy, differential scanning calorimetry (DSC) and X-ray diffraction (XRD). The results show that the compounds **3**, **4** and **5** exhibit a similar hexagonal liquid crystalline phase with a characteristic fan-shaped texture (Figure 2), whereas compounds **1** and **2** do not show any liquid crystalline phase. It is interesting to note that the transition temperature from the isotropic phase decreases as the carbon chain length increases (Table 1), which is consistent with the alkyl chain disordering effect to the columnar phase. For compound **3**, on first heating, the dark purple solid transforms into an isotropic liquid at 154.7°C with a transition enthalpy of ΔH=4.6 J g^{-1}. On cooling at a rate of 5°C min^{-1}, the compound first goes into a shearable liquid crystalline phase at 139.7°C (ΔH=1.1 J g^{-1}), which is characterized by the growth of distinct fan-shaped domains. This pattern is characteristic of the formation of a hexagonal columnar phase (Figure 2). On further cooling, another phase with high viscosity is formed at 137.0°C (ΔH=3.9 J g^{-1}), which persists through room temperature. In the phase below 137.0°C the texture of the hexagonal columnar phase remains unchanged, but with positional order along the columns.

The LC materials **3**, **4** and **5** are fluid in the isotropic phase and can be capillary-filled into thin cells. Very surprisingly, in films thinner than 10 μm the textures that appear on cooling at a rate slower than 2°C min^{-1} are almost completely black between crossed polarizers, indicating that the columns formed by strong intermolecular self-assembly are perpendicularly aligned to the film substrates, i.e. homeotropic alignment (Figure 3). This behaviour is very important because it provides a pathway to obtain defect-free crystalline thin film by cooling the well-aligned LC phase at a specific rate. XRD obtained from an optically dark homeotropic monodomain in a thin

Table 1. Phase transition temperatures (°C) and enthalpies (J g^{-1}, in parentheses) on cooling at 5°C min^{-1} for compounds **1**–**5**.

Compound	Phase transitions
1	I 166.8 (12.7) Cr
2	I 162.3 (13.8) Cr
3	I 139.7 (1.1) Col_h 137.0 (7.7) Col_{ho} < −50 Cr
4	I 135.4 (2.5) Col_h 115.7 (7.3) Col_{ho} −14 (10.0) Cr
5	I 121.0 (1.9) Col_h 96.7 (5.8) Col_{ho} −9.7 (23.0) Cr

I=isotropic liquid; Col_h=hexagonal LC phase; Col_{ho}=(ordered) hexagonal LC phase; Cr=crystal.

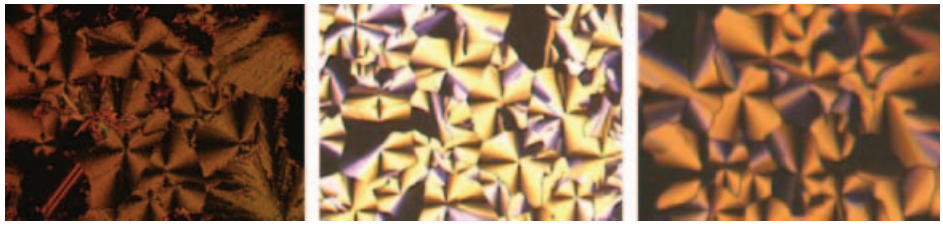

(a) (b) (c)

Figure 2. Crossed-polarized optical textures of (a) **3** at 132°C, (b) **4** at 115°C and (c) **5** at 117°C.

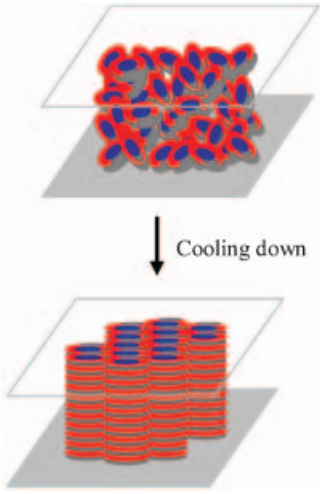

Figure 3. Schematic diagram of homeotropic alignment of **3**, **4** and **5** upon cooling from the isotropic phase.

film confirms the homeotropically aligned crystal phase in which the molecules stack into columns forming a hexagonal lattice. Figure 4 shows the XRD patterns from the isotropic phase of **3** and homeotropically aligned thin films of **3** and **4**. The *d*-spacing between two columns (centre to centre) is 4.19 nm and the *d*-spacing between two molecules in a column for π–π stack is 0.34 nm in Figure 4B.

Polarized optical textures of **3** in homeotropically aligned cells at room temperature with 2 µm and 8 µm samples both with ITO–ITO and ITO–gold electrode pairs are shown in Figure 5. It can be seen that the alignment of the material in all four of the cells tends to be homeotropic. Thinner films with 2 µm thickness in Figures 5b and 5d have almost perfect homeotropic alignment. Moreover, the alignment of the phase remains stable through room temperature down to –50°C. It is worth noting that the exceptionally spontaneous formation of homeotropic alignment results from the unique fluid (disordered) hexagonal columnar phases of these materials. It is extremely important for photovoltaic application since it is the most favourable molecular arrangement providing the most efficient path for electrons and holes along the columnar axis, and the light harvesting molecules are arranged with the largest areas toward the incoming light (Figure 3). To the best of our knowledge, these LC materials are the first light-harvesting liquid crystalline porphyrins in which homeotropic alignment has been achieved.

The time dependences of the induced currents in **3** homeotropically aligned thin film cells are shown in Figure 6 (right), for light of 1.8 mW mm^{-2} intensity turned OFF and ON. Both the build-up and decay of the electric current take about 2 s. The current induced in 1 mm^2 areas is about an order of magnitude larger for the 2 μm cells than for the 8 µm cells for both ITO–ITO and ITO–gold electrode pairs. The 2 µm cells have much larger efficiency than that of the 8 µm cells. The increase of the efficiency can mainly be ascribed to the improved alignment. It is also seen that the efficiency of the 2 µm cell with ITO–gold electrode pairs is more than twice as large as that of the 2 µm cell with ITO–ITO electrodes.

Photoconversion in the thick films studied might be due to only surface effects and the charges are coming only from a few nanometres below the surface in the bulk. At the electrode and photovoltaic material surface, the different electron affinity causes electron transfer or energy band alignment and induces charge separation. For ITO–ITO cell construction, this charge separation effect does not occur on the non-irradiated electrode, and the net electromotive force is produced by the concentration difference at the two electrodes. Experiment shows that the illuminated electrode is the anode, which is consistent with this proposed mechanism. For

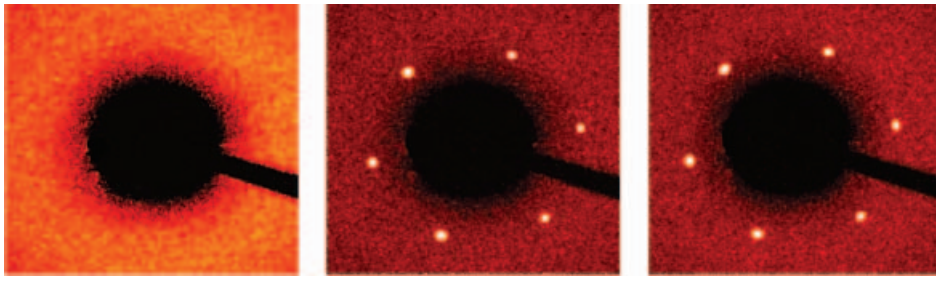

(a) (b) (c)

Figure 4. Synchrotron X-ray diffraction patterns from the (A) isotropic phase (142°C) and (B) homeotropic monodomain (136°C) of **3**, and (C) the homeotropic monodomain of **4** (100°C) (sample sandwiched between 50 µm thick bare glass substrates with 8 µm gap).

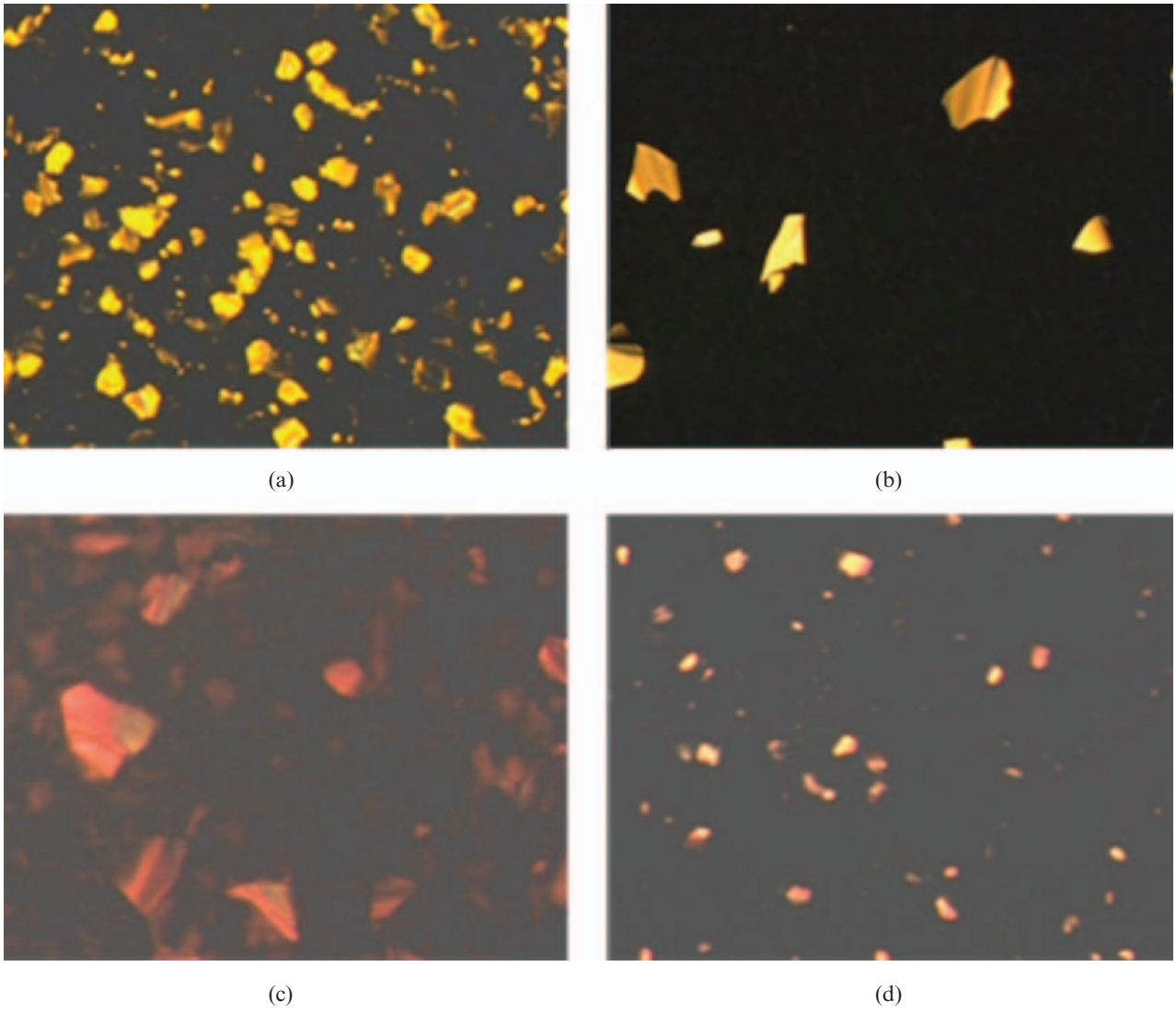

Figure 5. Crossed-polarized optical textures of **3** in homeotropically aligned cells (the dark areas represent homeotropic alignment where the planes of the disk-shaped molecules are parallel to the substrates). Bright domains represent areas where the molecular planes are tilted with respect to the substrates. (a) 8 µm ITO–ITO cell; (b) 2 µm ITO–ITO cell; (c) 8 µm ITO–gold cell; (d) 2 µm ITO–gold cell. The pictures represent 0.3 mm × 0.2 mm areas.

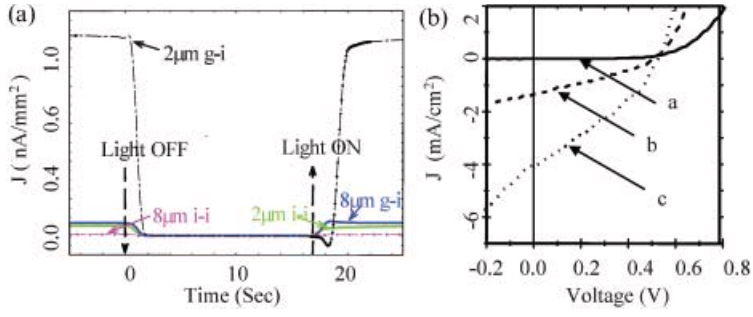

Figure 6. (a) Time dependences of the induced currents in normalized current density per 1 mm^2 area in **3** homeotropically aligned thin-film cells (g-i: gold–ITO; i-i: ITO–ITO electrode pairs). The light source was a mercury lamp. The area of the cell was measured directly. (b) *J–V* characteristics of the bulk-heterojunction solar cells based on **3** (a: in the dark; b: under illumination of AM 1.5G, 100 mW cm^{-2}; c: cooling to room temperature after heating the cell to 145°C, then under illumination of AM 1.5G, 100 mW cm^{-2}).

ITO–gold construction, the difference in the work function of the two electrodes brings more non-symmetry to the system, thus facilitating charge separation. This effect may also be augmented by the decreasing light intensity across the film (2 μm cells absorb about 30% of the visible light). The generated power and the efficiency of the studied cells of the pure porphyrin material without doping with electron acceptors is low since the diffusion length of the excitons are about 10 nm (*13*), i.e. three orders of magnitude less than the film thickness. Together with the fact that the surface homeotropic alignment becomes more and more effective with decreasing thickness, we can expect improvements in efficiency when using thinner film.

In order to understand the photovoltaic properties of the materials, the preliminary photovoltaic performance of material **3** was investigated based on bulk-heterojunction solar cells, which were fabricated by sandwiching a blend film of porphyrin **3** and PCBM (a C_{60} derivative) (1:1 w/w) between the ITO anode coated with a conductive polymer poly(3, 4-ethylenedioxythiophene) (PEDOT) and Ca/Al cathode. In such solar cells, porphyrin acts as an electron donor, whereas PCBM acts as an electron acceptor. Post annealing was carried out by heating the solar cells on a hot stage from room temperature (~25°C) to ~140°C and held for ~10 min, followed by subsequent cooling down from 140°C to 80°C with an average cooling rate of 0.2°C min^{-1} and from 80°C to room temperature with a cooling rate of 5°C min^{-1}. Figure 6 (right) shows current density versus voltage (*J–V*) characteristics of the bulk-heterojunction solar cells before and after the post-annealing, respectively, under the illumination of AM 1.5G, 100 mW cm^{-2}. The as-prepared device exhibited an open circuit voltage (V_{oc}) of 0.510 V, a short circuit current density (J_{sc}) of 1.340 mA cm^{-2} and power conversion efficiency (PCE) of 0.222%. Device performance was improved significantly by about 300–400% increase in J_{sc} and PCE, respectively, by the post-annealing treatment. The post-annealed device achieved a J_{sc} of 3.99 mA cm^{-2} and a PCE of 0.712%. The post-annealing induced device performance enhancement in the bulk-heterojunction solar cells was attributable to the better alignment of the porphyrins. The preliminary photovoltaic performance is inspiring since a homeotropic alignment is very difficult to achieve in the blend film of porphyrin **3** and PCBM (1:1 w/w). We can anticipate dramatic improvements in efficiency by tailoring optimal cell structure and engineering if we can maintain the homeotropically aligned architecture in bulk-, double- or multi-heterojunction solar cells.

4. Conclusions

We present here a new class of nanoscale liquid crystalline porphyrins, which have the basic structure inspired by natural light-harvesting materials. These materials can be exceptionally homeotropically aligned into a highly ordered nanostructure in which the columns formed by intermolecular π–π stacking are spontaneously perpendicular to the film substrate. The homeotropic alignment, well confirmed by synchrotron X-ray diffraction, is extremely important for photovoltaic applications since the most favourable molecular arrangement can provide the most efficient path for electrons and holes along the columnar axis, and the light-harvesting molecules are arranged with the largest area toward the coming light. Their preliminary photocurrent generation and photovoltaic performance were also demonstrated. This work shows the essence of nanotechnology in which core issue is self-assembly due to the large conjugation system of porphyrin together with the unique properties of liquid crystals. The results provide some insight on the development of organic photovoltaics by using homeotropically aligned liquid crystal thin film.

Acknowledgements

This work was supported, in part, by LCI, an Ohio Board of Regents' Research Challenge award, AFOSR (FA9550-06-1-0384) and National Science Foundation grant DMR-0637221. Use of the Advanced Photon Source (APS) was supported by the US Department of Energy (DOE), Basic Energy Sciences (BES), Office of Science, under Contract No. W-31-109-Eng-38. The Midwestern Universities Collaborative Access Team's (MUCAT) sector at the APS is supported by the US DOE, BES, Office of Science, through the Ames Laboratory under Contract No. W-7405-Eng-82.

References

(1) Bard A.J.; Stratmann M.; Licht S. *Semiconductor Electrodes and Photoelectrochemistry: Volume of Encyclopaedia of Electrochemistry*; Wiley-VCH: Darmstadt, 2002.
(2) Grätzel M. *Nature* **2001**, *414*, 338–344.
(3) Wöhrle D.; Meissner D. *Adv. Mater.* **1991**, *3*, 129–138.
(4) Green M.A. *Third Generation Photovoltaics: Advance Solar Energy Conversion*; Springer-Verlag: Berlin, 2004.
(5) *Basic Research Needs for Solar Energy Utilization.* Report on the Basic Energy Sciences Workshop on Solar Energy Utilization, chaired by Lewis, N.S.; Crabtree, G., panel chaired by Nozik, A.J., Wasielewski, M.R. & Alivisatos, P., April 18–21, 2005, Office of Science, US Department of Energy.
(6) Colling P.J.; Hird M., *Introduction to Liquid Crystals, Chemistry and Physics*; Taylor & Francis: London, 1997; Wang, Q.-M.; Bruce, D.W. *Chem. Commun.*

1996, *22*, 2505–2506; Adams, D.; Schuhmacher, P.; Simmerer, J.; Haussling, L.; Siemensmeyer, K.; Etzbach, K.H.; Ringsdorf, H.; Haarer, D. *Nature* **1994,** *371,* 141–143.

(7) Hazuaki H.; Ohta K.; Yamamoto I.; Shirai H. *J. Mater. Chem.* **2001**, *11*, 423–433; Schmidt-Mende, L.; Fechtenkötter, A.; Müllen, K.; Moons, E.; Friend, R.H.; MacKenzie, J.D. *Science* **2001,** *293,* 1119–1122; Schmidt-Mende, L.; Watson, M.; Müllen, K.; Friend, R.H. *Mol. Cryst. liq. Cryst.* **2003,** *396,* 73–90; Grelet, E.; Bock, H. *Europhys. Lett.* **2006,** *73,* 712–718; Pisula, W.; Tomovic, Z.; El Hamaoui, B.; Watson, M.D.; Pakula, T.; Mullen, K. *Adv. funct. Mater.* **2005,** *15,* 893–904; Li, Q.; Li, L. In *Thermotropic Liquid Crystals*; Ramamoorthy, A., Ed.; Springer: Berlin, 2007.

(8) Eichhorn H.J. *Porphyrins Phthalocyanines* **2000**, *4*, 88–102; Shimizu, Y.; Miya, M.; Nagata, A.; Ohta, K.; Yamamoto, I.; Kusabayashi, *S. Liq. Cryst.* **1993,** *14,* 795–805.

(9) Goodby J.W.; Robinson P.S.; Teo B.K.; Cladis P.E. *Mol. Cryst. liq. Cryst. Lett.* **1980**, *56*, 303–309.

(10) Gregg B.A.; Fox M.A.; Bard A.J. *J. Am. chem. Soc.* **1989**, *111*, 3024–3029; Gregg, B.A.; *Mol. Cryst. liq. Cryst.* **1994,** *257* 219–227; Liu, C.-Y.; Pan, H.-L.; Fox, M.-A.; Bard, A.J. *Science* **1993,** *261,* 897–899; Liu, C.-Y.; Bard, A.J. *Nature* **2002,** *418,* 162–164.

(11) Fox M.A.; Grant J.V.; Melamed D.; Torimoto T.; Liu C.-Y.; Bard A.J. *Chem. Mater.* **1998**, *10*, 1771–1776.

(12) Kang S.-W.; Li Q.; Chapman B.D.; Pindak R.; Cross J.; Li L.; Nakata M.; Kumar S. *Chem. Mater.* **2007**, *19*, 5657–5663.

(13) Donker H.; van Hoek A.; van Schaik W.; Koehorst R.B.M.; Yatskou M.M.; Schaafsma T.J. *J. phys. Chem. B* **2005**, *109*, 17038–17046.